Journal of Materials Chemistry C

Electronic implications of organic nitrogen lone pairs in lead iodide perovskites

Journal:	*Journal of Materials Chemistry C*
Manuscript ID	TC-ART-01-2018-000376.R1
Article Type:	Paper
Date Submitted by the Author:	28-Mar-2018
Complete List of Authors:	Kasel, Thomas; University of Oregon, Chemistry and Biochemistry Hendon, Christopher; University of Oregon, Chemistry and Biochemistry

Journal Name

ARTICLE TYPE

Cite this: DOI: 10.1039/xxxxxxxxxx

Electronic implications of organic nitrogen lone pairs in lead iodide perovskites†

Thomas W. Kasel[a] and Christopher H. Hendon[a,*]

Received Date
Accepted Date

DOI: 10.1039/xxxxxxxxxx

www.rsc.org/journalname

Hybrid halide perovskites composed of protic organic A-site cations are promising materials for the conversion of light into electricity. Polycrystalline technologies are of particular interest because of their desirable processability, but suffer from decreased efficiency compared to single crystal devices, in part owing to trap states at grain boundaries. Recent remedies for increasing performance of polycrystalline lead iodide-based perovskites include the addition of organic polymers at grain boundaries, serving to both prevent material decomposition and passivate the grain. Here we demonstrate that, using the 2D perovskite architecture as an analogue for the 3D material, passivating layers containing nitrogen lone pairs may act as chromophores, resulting in poor material performance.

Introduction

Over the past decade lead iodide-based perovskite solar cell architectures have become a major research focus owing to advances in their efficiency to convert light into electricity[1–6]. The archetypal material methylammonium lead iodide ($CH_3NH_3PbI_3$) boasts several advantages over other solar technologies, including its rapid and scalable synthesis, and cheap processing. However, the protic nature of $CH_3NH_3^+$ and other ammonium- and iminium-based organohalide perovskites[7–10] is one origin of thermal and moisture instability, causing decomposition (Figure 1a)[11–17]. This combined with the polycrystalline architecture[18,19] results in the numerous crystal faces acting as both a source of electron traps and sites for decomposition.

One approach towards improving $CH_3NH_3PbI_3$ stability has been through compositional modification. Some success has been found through substitutions of the organic cation, as the pK_a of the N-bound protons (and therefore the reactivity with water) is determined by the stability of the N-centered cation[20,21]. However, only a handful of organic cations are small enough to fit in the PbI_3^- cage, limiting the material's modularity[22]. The elec-

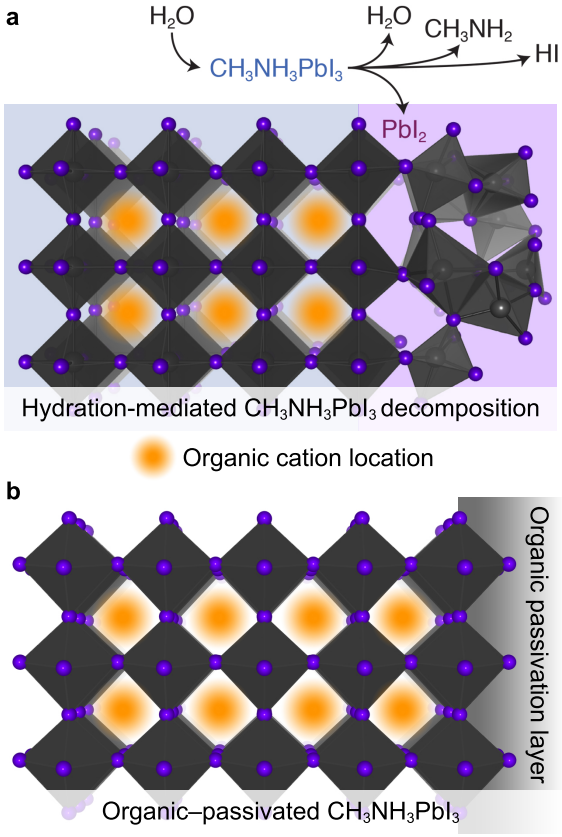

Fig. 1 a) The organic motif in protic organohalide perovskites (orange) reacts with water to form methylamine, CH_3NH_2 evaporates at low temperatures, forming PbI_2 and residual HI. b) The addition of a hydrophobic passivation agent at either external device faces or at grain boundaries is thought to improve moisture stability. They also act as a physical barrier to imminent water. Lead and iodine are shown in grey and eminence respectively.

[a]*Department of Chemistry and Biochemistry, University of Oregon, Eugene, OR, 97401, USA. Twitter: @chhendon; Tel: +1 541 346 2637; E-mail: chendon@uoregon.edu*

† Electronic Supplementary Information (ESI) available: Geometrically optimized structure files, computed optical absorption spectra, and complete electronic band structure of $(PMA)_2PbI_4$ See DOI: 10.1039/b000000x/

tronic properties of PbI_3^--based materials remain largely independent of the organic cation.

The most successful approach for maximizing stability of hybrid PbI_3^- systems has been to quite simply keep the material dry. Surface passivation – both crystallographic[23] and at grain boundaries[24,25] – with hydrophobic organic molecules have shown some early success[26] (a (100) passivation is shown schematically in Figure 1b). Passivating agents incorporated at grain boundaries have been shown to increase device stability, prolonging device lifetimes[27] presumably slowing water penetration into the material.

Organic passivating agents are typically composed of polymers containing tertiary amines (formed through ammonia condensation polymerization), as well as other non-polar polymers. The shortcoming of this approach is that the passivating agents potentially decrease device efficiency as the organic polymers are not typically electrically conductive.

Results and Discussion

Our initial motivation was to examine the electronic implications of direct A-site substitution for a polymeric organic cation, which we conjecture would serve to mitigate water instability. Polymeric cations could potentially overcome entropic decomposition of $CH_3NH_3PbI_3$ through a hydration-mediated deprotonation and subsequent release of CH_3NH_2. We elected to use polymers containing alkaline heteroatoms which could be protonated to form a charge neutral solid, as they were most reminiscent of methylammonium itself (*e.g.* aliphatically linked tertiary amines) one example shown in Figure 3f. After careful construction and optimization of several representative aliphatic cationic-polymer-PbI_3 models the resultant materials were determined to be unstable. The aliphatic -CH_2-CH_2- is too large to fit through the face of the perovskite resulting in significant Peirels distortion of the PbI_6 octahedron. Although this outcome was unsurprising as syntheses involving large organic cations typically yield a 2D perovskite structure type.

During that initial investigation we noted one subtle utility of the 2D perovskite structure-type: they are reasonable models for the most extreme 3D perovskites grain boundary (a monolayer of anionic lead iodide). This similarity arises because the 2D PbI_4^{2-} and the (100) surface of the 3D PbI_3^- have analogous dangling iodides, Figure 2a, thus allowing us to model a surface without having to cleave a dipole neutral surface of the parent 3D semiconductor[28,29]. The validity of this surface approximation is predicated on the fact that dangling monolayer 2D iodides are less stable (*i.e.* higher energy) than their 3D counterparts due to the increase charge density of the PbI_4^{2-} sheet. Of course, other 2D PbI_n materials have been reported[30], and could also be used in a similar fashion to analyze the electronic influences of the organic passivating agents on the electronic properties at grain boundaries of 3D materials.

The confinement of the 2D Pb-I connectivity manifests as a reduction in electronic band curvature and minor increase in band gap, as evidence by comparison of electronic band structures in Figure 2b. These effects are inconsequential for the subsequent examination of the impact of organic functional groups on the frontier bands, as the 2D PbI_4^{2-} 'surface' should be an energetically conservative model of the 3D system 'surface' allowing for us to compare perturbations to the valence band maximum (VBM) and conduction band minimum (CBM) of the 2D material.

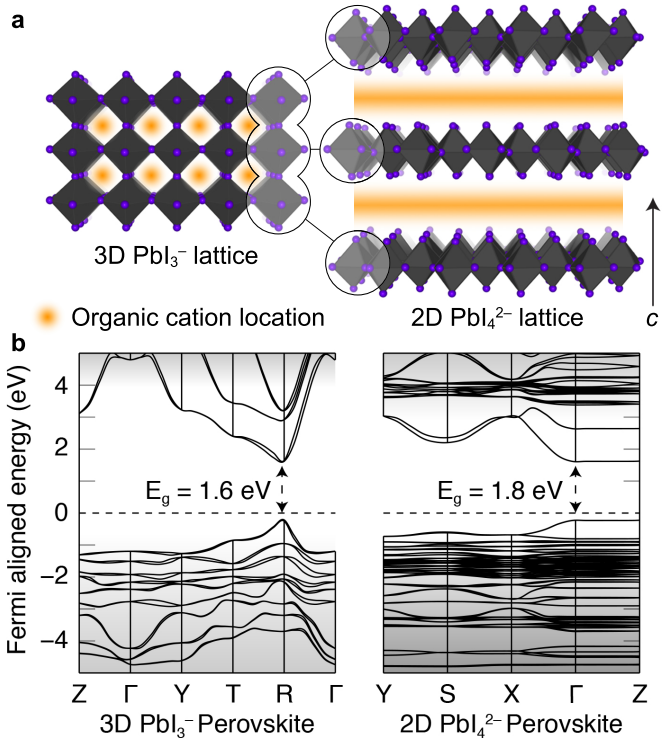

Fig. 2 a) The 3D perovskite PbI_3^- cage features similar inorganic connectivity to the 2D PbI_4^{2-} counterpart. The 2D dangling iodides are analogous to the (100), (010), and (001) surfaces of the 3D material. b) The electronic band structure of the 3D material features large band curvature in the conduction band, associated with delocalized Pb *p*-states. The valence band has less dispersion, and is comprised of a combination of Pb *s*- and I *p*-states. The reduction in Pb-I dimensionality in the 2D perovskite results in reduced curvature in both band extrema. Special points map to P*m-3m* and P*bca* space groups for the 3D and 2D structures, respectively.

Using computational methods, this study details the utility of the 2D perovskite architecture in assessing the electronic implications of both i) the organic cation in the bulk 2D system, as well as ii) passivation agents at grain boundaries in the larger family of 3D PbI_3^--based materials. Using the 2D model we show that organic layers containing nitrogen lone pairs are expected to act as a chromophore (installing a new flat valence band) composed of N p-states, highlighting the potential photochemical non-innocence of common organic passivation agents.

Starting with a representative 2D perovskite, phenylmethylammonium lead iodide ($(PMA)_2PbI_4$)[31], the electronic band structure, Figure 3a, was generated using the Computational Method. The Z-Γ vector is decidedly flat, corresponding to sampling in the crystallographic *c* direction (the direction with no covalent Pb-I connectivity, Figure 2a). $(PMA)_2PbI_4$ features a direct band gap of 1.8 eV at the Γ point, closely matching the experimental report[31]. Optical absorption spectra are presented in the Electronic Supplementary Information. Large band curvature is observed in

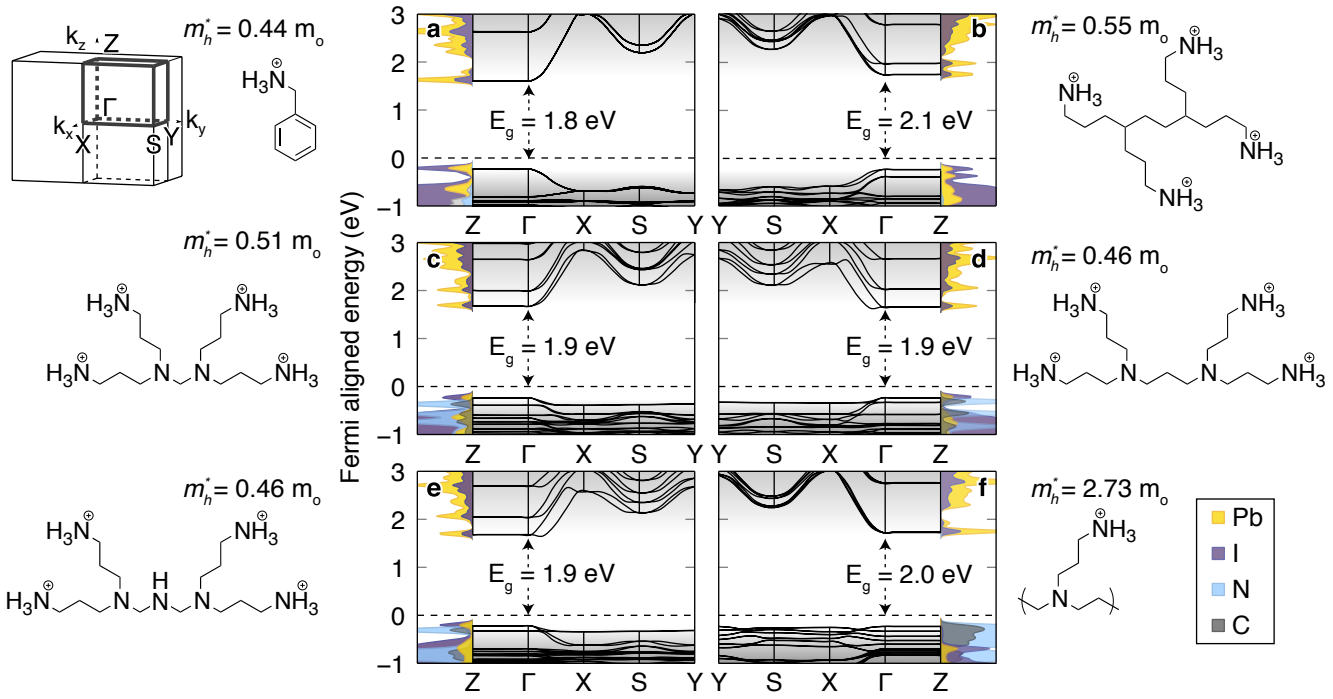

Fig. 3 Electronic band structures and density of states (DOS) of 2D perovskites with their corresponding organic cations. The **k**-vectors map to space group P*bca*, and the first Brillouin zone is shown. All electronic structures were computed using PBEsol+SOC. DOS is reported for *Gamma* only. Organic molecules containing nitrogen lone pairs show nitrogen DOS near the VBM, which grows with increasing concentration of tertiary nitrogen.

the direction of Pb-I connectivity, where the VBM and CBM are composed of primarily iodine and lead orbitals, respectively.

Perturbations to $(PMA)_2PbI_4$ were made by substituting PMA for aliphatic catonic ammonium polymers, Figure 3. Upon geometric equilibriation (details in Computational Methods) the electronic band structure of the system with only quaternary nitrogen (Figure 3b) show negligible perturbation, with both the curvature and composition of the bands remaining unchanged. The band structure does show reduced degeneracy owing to the asymmetric nature of the aliphatic carbon, reducing the cell to P*1*.

The experimentally relevant inclusion of tertiary amines in the backbone of the organic cation again yields a similar band gap and curvature in the conduction bands, Figure 3c-f. While the VBM remains unperturbed, the valence band shows the emergence of a highly localized nitrogen-based band which can be attributed to nitrogen lone pairs, Figure 3c-f. The flat band is unaffected by inter nitrogen chain length (as evidenced by Figure 3c and d). Increasing the concentration of lone pairs shows an increase in nitrogen density of states, Figure 3e, most extremely demonstrated by the inclusion of a polymer (Figure 3f). The nitrogen effect is further evidenced by the increase in hole effective mass ($m_h^* = 0.44\ m_o$ and $m_h^* = 2.73\ m_o$ for $(PMA)_2PbI_4$ and (polymer)PbI_4, respectively). All hole effective masses are presented in Figure 3. The polymer-containing material is most relevant as it belongs to the same family of materials used for grain boundary passivation of the 3D counterparts[24]. In this case, our polymer features one amine lone pair per ammonium tail and the band structure shows a significant contribution to the valence DOS from the amine group, suggesting that the lone pair should be a chromophore.

Conclusion

The emergence of nitrogen lone pairs to the valence band is concerning because the hole mobility of the material is directly determined by the valence band curvature. Remembering that the 2D VBM is likely higher in energy than the 3D surface, this is of particular concern because this could result in nitrogen lone pairs sitting midgap at a grain boundary of the 3D architecture.

In summary we concisely demonstrated that nitrogen lone pairs may be chromophores in PbI_n-based materials. Furthermore we also show that the 2D architectures are reasonable models for surfaces of 3D perovskites, allowing us to probe the electronic properties of relevant surfaces and grain boundaries. Beyond the results presented herein, we hope to have demonstrated the utility of the 2D architectures for further computational studies on the effects of organic substituents used in both 2D and 3D PbI_n-based materials.

Computational Methods

Beginning with the experimentally determined structure of the 2D perovskite phenylmethylammonium lead iodide[31], the organic cation was substituted for alternative aliphatic cations with protonation states adjusted for stoichiometric charge neutrality. The resultant materials were then geometrically equilibriated using the DFT functional PBEsol[32], as implemented in VASP[33]. A 500 eV planewave cutoff and a 3x3x1 **k**-grid was determined to provide satisfactory convergences to within 0.005 eV per atom.

Spin-orbit coupling (SOC) is required to recover the accurate electronic structure of materials containing lead and iodine. Al-

though HSE06 + 43% HF exchange + SOC has been shown to produce the correct electronic band gap and curvature, we cannot apply this to the 2D system due to computational expense. Instead, we note that PBEsol without SOC is found to recover the correct band gap through a systematic underestimation of band gaps: PBEsol+SOC underestimates the electronic band gap. Hence, the electronic structure presented in this paper uses the band structures computed with PBEsol+SOC with the conduction band energies adjusted to reflect the PBEsol band gap. Given the Pb-I connectivity was largely unaltered by the organic substitutions, we computed the electronic band structure using high symmetry points that map to the parent space group of the literature phenylmethylammonium lead iodide material, P*bca*. Effective masses were calculated from VBM curvature recovered from a high resolution scan around Γ. Absorption spectra were computed from single point electronic calculations.

The electronic band structure of the 3D material was produced using the orthorhombic structure optimized using PBEsol, a 6x6x6 **k**-grid and 500 eV cutoff. The electronic band structure was produced using the same procedure as above.

Acknowledgments

This work used the Extreme Science and Engineering Discovery Environment (XSEDE), which is supported by National Science Foundation grant number ACI-1548562.

Conflict of interest

There are no conflicts to declare.

References

1 A. Kojima, K. Teshima, Y. Shirai and T. Miyasaka, *J. Am. Chem. Soc.*, 2009, **131**, 6050–6051.
2 G. E. Eperon, G. M. Paternò, R. J. Sutton, A. Zampetti, A. A. Haghighirad, F. Cacialli and H. J. Snaith, *J. Mater. Chem. A*, 2015, **3**, 19688–19695.
3 H.-S. Kim, C.-R. Lee, J.-H. Im, K.-B. Lee, T. Moehl, A. Marchioro, S.-J. Moon, R. Humphry-Baker, J.-H. Yum, J. E. Moser, M. Grätzel and N.-G. Park, *Sci. Rep.*, 2012, **2**, 591.
4 Y. Wu, D. Yan, J. Peng, T. Duong, Y. Wan, P. Phang, H. Shen, N. Wu, C. Barugkin, X. Fu, S. Surve, D. Walter, T. White, K. Catchpole and K. Weber, *Energy Environ. Sci.*, 2017, **11**, 2472–2479.
5 Q. Jiang, Z. Chu, P. Wang, X. Yang, H. Liu, Y. Wang, Z. Yin, J. Wu, X. Zhang and J. You, *Adv. Mater.*, 2017, **29**, 1703852.
6 Y. Wu, F. Xie, H. Chen, X. Yang, H. Su, M. Cai, Z. Zhou, T. Noda and L. Han, *Adv. Mater.*, 2017, **29**, 1701073.
7 Y. Zong, Y. Zhou, M. Ju, H. F. Garces, A. R. Krause, F. Ji, G. Cui, X. C. Zeng, N. P. Padture and S. Pang, *Angew. Chem. Int. Ed.*, 2016, **55**, 14723–14727.
8 Z. Wang, Q. Lin, F. P. Chmiel, N. Sakai, L. M. Herz and H. J. Snaith, *Nat. Energy*, 2017, **2**, 17135.
9 N. De Marco, H. Zhou, Q. Chen, P. Sun, Z. Liu, L. Meng, E.-P. Yao, Y. Liu, A. Schiffer and Y. Yang, *Nano Lett.*, 2016, **16**, 1009–1016.
10 C. C. Stoumpos, L. Frazer, D. J. Clark, Y. S. Kim, S. H. Rhim, A. J. Freeman, J. B. Ketterson, J. I. Jang and M. G. Kanatzidis, *J. Am. Chem. Soc.*, 2015, **137**, 6804–6819.
11 E. J. Juárez-Pérez, Z. Hawash, S. Ruiz Raga, L. Ono and Y. Qi, *Energy Environ. Sci.*, 2016, **9**, 3406–3410.
12 B. Conings, J. Drijkoningen, N. Gauquelin, A. Babayigit, J. D'Haen, L. D'Olieslaeger, A. Ethirajan, J. Verbeeck, J. Manca, E. Mosconi, F. D. Angelis and H.-G. Boyen, *Adv. Energy Mater.*, 2015, **5**, 1500477.
13 Z. Song, A. Abate, S. C. Watthage, G. K. Liyanage, A. B. Phillips, U. Steiner, M. Graetzel and M. J. Heben, *Adv. Energy Mater.*, 2016, **6**, 1600846.
14 E. Mosconi, J. M. Azpiroz and F. De Angelis, *Chem. Mater.*, 2015, **27**, 4885–4892.
15 A. Dualeh, P. Gao, S. I. Seok, M. K. Nazeeruddin and M. Grätzel, *Chem. Mater.*, 2014, **26**, 6160–6164.
16 Q. Sun and W.-J. Yin, *J. Am. Chem. Soc.*, 2017, **139**, 14905–14908.
17 J. M. Frost, K. T. Butler, F. Brivio, C. H. Hendon, M. van Schilfgaarde and A. Walsh, *Nano Lett.*, 2014, **14**, 2584–2590.
18 W. Nie, H. Tsai, R. Asadpour, J.-C. Blancon, A. J. Neukirch, G. Gupta, J. J. Crochet, M. Chhowalla, S. Tretiak, M. A. Alam, H.-L. Wang and A. D. Mohite, *Science*, 2015, **347**, 522–525.
19 O. G. Reid, M. Yang, N. Kopidakis, K. Zhu and G. Rumbles, *ACS Energy Lett.*, 2016, **1**, 561–565.
20 T. W. Kasel, A. T. Murray and C. H. Hendon, *J. Phys. Chem. C*, 2018, **122**, 2041–2045.
21 G. E. Eperon, S. D. Stranks, C. Menelaou, M. B. Johnston, L. M. Herz and H. J. Snaith, *Energy Environ. Sci.*, 2014, **7**, 982–988.
22 G. Kieslich, S. Sun and A. K. Cheetham, *Chem. Sci.*, 2015, **6**, 3430–3433.
23 I. Hwang, I. Jeong, J. Lee, M. J. Ko and K. Yong, *ACS Appl. Mater. Interfaces*, 2015, **7**, 17330–17336.
24 L. Zuo, H. Guo, D. W. deQuilettes, S. Jariwala, N. D. Marco, S. Dong, R. DeBlock, D. S. Ginger, B. Dunn, M. Wang and Y. Yang, *Sci. Adv.*, 2017, **3**, 1700106.
25 X. Zheng, B. Chen, J. Dai, Y. Fang, Y. Bai, Y. Lin, H. Wei, X. C. Zeng and J. Huang, *Nat. Energy*, 2017, **2**, 17102.
26 L. Iagher and L. Etgar, *ACS Energy Lett.*, 2018, **3**, 366–372.
27 M. Xiao, F. Huang, W. Huang, Y. Dkhissi, Y. Zhu, J. Etheridge, A. Gray-Weale, U. Bach, Y.-B. Cheng and L. Spiccia, *Angew. Chem. Int. Ed.*, 2014, **126**, 10056–10061.
28 F. Finocchi, A. Barbier, J. Jupille and C. Noguera, *Phys. Rev. Lett.*, 2004, **92**, 136101.
29 A. J. Logsdail, D. O. Scanlon, C. R. A. Catlow and A. A. Sokol, *Phys. Rev. B*, 2014, **90**, 155106.
30 C. C. Stoumpos, D. H. Cao, D. J. Clark, J. Young, J. M. Rondinelli, J. I. Jang, J. T. Hupp and M. G. Kanatzidis, *Chem. Mater.*, 2016, **28**, 2852–2867.
31 M. E. Kamminga, H.-H. Fang, M. R. Filip, F. Giustino, J. Baas, G. R. Blake, M. A. Loi and T. T. M. Palstra, *Chem. Mater.*, 2016, **28**, 4554–4562.
32 J. P. Perdew, A. Ruzsinszky, G. I. Csonka, O. A. Vydrov, G. E. Scuseria, L. A. Constantin, X. Zhou and K. Burke, *Phys. Rev. Lett.*, 2008, **100**, 136406.
33 G. Kresse and J. Furthmüller, *Phys. Rev. B*, 1996, **54**, 11169–11186.

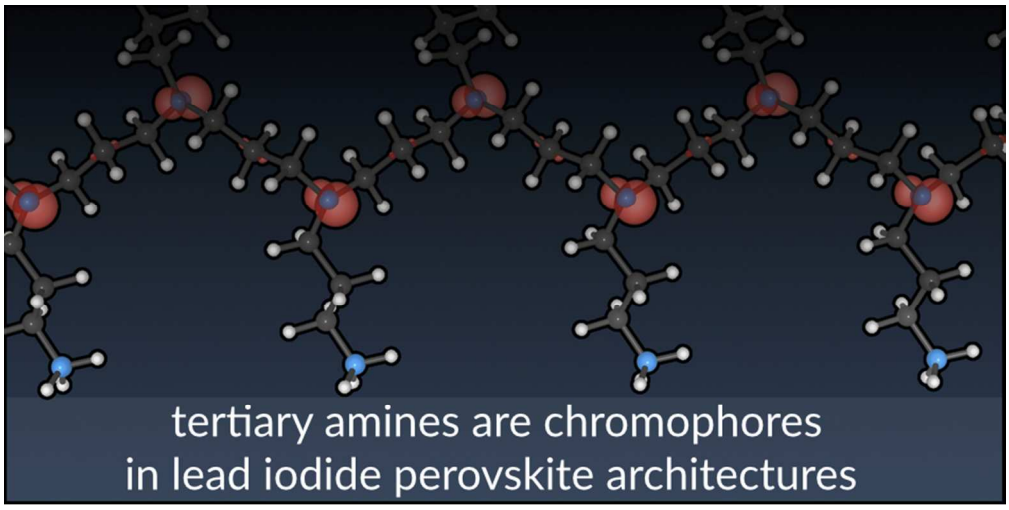
tertiary amines are chromophores
in lead iodide perovskite architectures